Mathematics

AIMS Mathematics, 6(10): 10861–10880.
DOI: 10.3934/math.2021631
Received: 17 January 2021
Accepted: 16 July 2021
Published: 28 July 2021

http://www.aimspress.com/journal/Math

Research article

Impact of estrogen population pharmacokinetics on a QSP model of mammary stem cell differentiation into myoepithelial cells

Justin Le Sauteur-Robitaille[1,2], Zhe Si Yu[1] and Morgan Craig[1,2,*]

[1] Département de mathématiques et de statistique, Université de Montréal, Montréal, QC, Canada
[2] Sainte-Justine University Hospital Research Centre

*** Correspondence:** Email: morgan.craig@umontreal.ca; Tel: +15143437471; Fax: +15143435700.

Abstract: Stem cell differentiation cascades are critical components of healthy tissue maintenance. Dysregulation in these systems can lead to serious diseases, including cancer. Myoepithelial mammary cells are produced from differentiated mammary stem cells in processes regulated, in part, by estrogen signalling and concentrations. To quantify and predict the production of mammary myoepithelial cell production by estrogen, we developed a mechanistic, quantitative systems pharmacology (QSP) model that includes the explicit characterization of free and unbound estrogen concentrations in circulation. Linking this model to a previously developed population pharmacokinetics model for ethinyl estradiol, a synthetic form of estrogen included in oral contraceptives, we predicted the effects of estrogen on myoepithelial cell development. Interestingly, pharmacokinetic intraindividual variability alone did not significantly impact on our model's predictions, suggesting that combinations of physiological and pharmacokinetic variability drive heterogeneity in mechanistic QSP models. Our model is one component of an improved understanding of mammary myoepithelial cell production and development, and our results support the call for mechanistically constructed systems models for disease and pharmaceutical modelling.

Keywords: mammary myoepithelial cells; mammary stem cells; quantitative systems pharmacology; estrogen; pharmacokinetic variability; breast cancer
Mathematics Subject Classification: 92B05, 92C32

1. Introduction

Stem cell (SC) differentiation cascades are critical components of cellular and tissue maintenance [1]. SCs are pluripotent, largely quiescent, populations that repopulate terminally differentiated cells to maintain the latter's basal concentrations. This continuous and progressive differentiation scheme is regulated through cytokine and hormonal signals that control the proliferation and maturation of progenitor cell populations. One of the best understood SC systems is the hematopoietic compartment, which has been extensively studied since the 1960s [2,3]. Hematopoietic stem cells (HSCs) sit at the apex of the blood system and produce some 100 billion blood cells per day [4] in a remarkably regulated hierarchical (or quasi-hierarchical) structure. In the hematopoietic system, and other SC compartments, perturbations to this finely controlled signalling cascade are responsible for a number of diseases, including complex diseases [5]. For example, myelosuppression (lack of myeloid cells) due to cancer chemotherapy is a well-known consequence of cytotoxic anti-cancer treatments [6,7]. Thus, many mathematical models have been conceived to better understand the biology of myeloid cell production from HSCs to predict how patients will be affected by drug therapy [6,8–10].

Given the (intended or unintentional) influence of drugs on signalling networks, it is unsurprising that pharmaceutical scientists have long been interested in using mathematical modelling during preclinical and post-market planning to assess a drug's action at the target site and to forecast potential adverse events [11]. Historically, the pharmaceutical sciences have been concerned with empirical, mixed-effects models that can distinguish sources of variability within data, but which are limited in their ability to establish mechanistic relationships at the heart of drug effects [12]. In response, quantitative systems pharmacology (QSP) has emerged as a discipline concentrated on developing physiological systems models that, when linked to pharmacokinetics/pharmacodynamics (PK/PD), provide a holistic understanding of how drugs work [13]. In turn, the broader adoption of QSP has illustrated how cytokines regulate hematopoietic production and how best to schedule exogenous cytokines during chemotherapy [6,8–10], implement optimal dosing strategies for new cancer immunotherapies [14–18], and individualize drug schedules for children with attention deficit hyperactivity disorder [19], to name a few. There is therefore an increasing interest in applying QSP techniques to a broad set of unanswered physiological questions to provide a quantitative understanding of regulation within SC systems.

Estrogen is a broadly acting, primary female sex hormone that is also implicated in the regulation of mammary cells. Within the mammary differentiation program, estrogen signalling plays a role in the maintenance of the mammary stem cell (MaSC) population, differentiation into the various types of terminally differentiated mammary cells (myoepithelial, ductal, and alveolar) [20,21], and the downstream processes that produce each of these cell types. Mammary epithelium is a bilayer made up of an inner luminal layer and an outer basal myoepithelial layer [22]. A better understanding of the normal mammary cell differentiation program by signalling molecules inducing MaSC differentiation critical to provide a comprehensive view of normal regulation of the system, and interrogate how dysfunctionality caused by diseases such as breast cancer, the most common cancer and second leading cause of death amongst Canadian women [23], disrupts healthy regulatory processes and vice versa. Breast cancers are distinguished by the expression of certain receptors on mammary cells (i.e. estrogen, progesterone, and HER2). Breast cancer heterogeneity is driven by the plasticity of breast cancer cells that transition from epithelial-like (less aggressive, more treatable) to mesenchymal-like (more aggressive, more "stem"-like) [24]. This dedifferentiation (i.e. the change from more terminal to more stem-like cells) complicates therapy, is characteristic of more aggressive

cancers, and is regulated by hormones, including estrogen, progesterone, and prolactin [25]. However, stem and progenitor cells carry more proliferation potential than fully mature cells and breast cancer stem-like cells proliferation can be reduced by forcing tumour cells to differentiate through the use of hormones [26–29]. The use of QSP modeling can therefore help uncover the interactions regulating the dynamic evolution of mammary stem cells to provide a fundamental understanding that can subsequently be interpreted experimentally and clinically.

In this work, we leveraged our previous model of hematopoietic production regulated by cytokines [7] to propose a model of mammary stem cell differentiation into myoepithelial cells through estrogen signalling. Linking the model with the population PKs of ethinyl estradiol allowed us to investigate how heterogeneity in PKs affects mammary cell production. Our results suggest that our QSP modelling approach inherently incorporates pharmacokinetic variability in its construction, in line with our previous results in other stem cell differentiation cascades. These results underline the use of QSP models in normal and pathological systems to identify mechanisms of disease and provide guidance for drug administration and scheduling.

2. Methods

2.1. Mechanistic model of myoepithelial differentiation cascade regulated by estrogen

We constructed a physiological, QSP model describing the differentiation of mammary stem cells transitioning towards mature myoepithelial cells through estrogen regulation (Figure 1). Our model is based upon the classic G0 model of stem cells, originally developed to explain hematopoietic stem cell division [30] wherein stem cells are largely dormant, dividing to either self-renew or differentiate. In the mammary stem cell system, the emerging picture is that MaSCs largely lay dormant until puberty, with further lineage-restricted expansion during pregnancy [31]. Estrogen acts in a paracrine fashion to regulate differentiation of MaSCs into epithelial cells and certain ER+ luminal cells [20,31,32]. As a better understanding of mammary cell development is still unfolding, we adapted the stem cell models in [7,30] to study myoepithelial production from MaSCs.

Let $Q(t)$ be the concentration of mammary stem cells at time t, $M(t)$ the concentration of myoepithelial cells, $E_F(t)$ the concentration of free estrogen, and $E_b(t)$ the concentration of bound estrogen. Both free and bound estrogen concentrations were explicitly included as we have previously found that cytokine concentrations are not in quasi-equilibrium at homeostasis in the hematopoietic system [7].

Stem cell compartments maintain their populations through self-renewal via cell division. We therefore considered MaSCs that had divided τ_Q days ago to re-enter the compartment, and modelled the effective amplification resulting from self-renewing mitosis using

$$\mathrm{A_Q}\,(\mathrm{t}) = \mathrm{A_Q^*} = 2\mathrm{e}^{-\gamma_Q \tau_Q}, \tag{1}$$

where τ_Q is the time for cell division, γ_Q is the apoptotic rate during mitosis, and the factor of 2 accounts for the formation of two daughter cells from a single MaSC (symmetric cell division). The rate at which MaSCs enter the mitotic phase is given by

$$\beta(\mathrm{Q}) = \mathrm{f_Q}\,\frac{\theta_2^{s_2}}{\theta_2^{s_2} + \mathrm{Q}^{s_2}}, \tag{2}$$

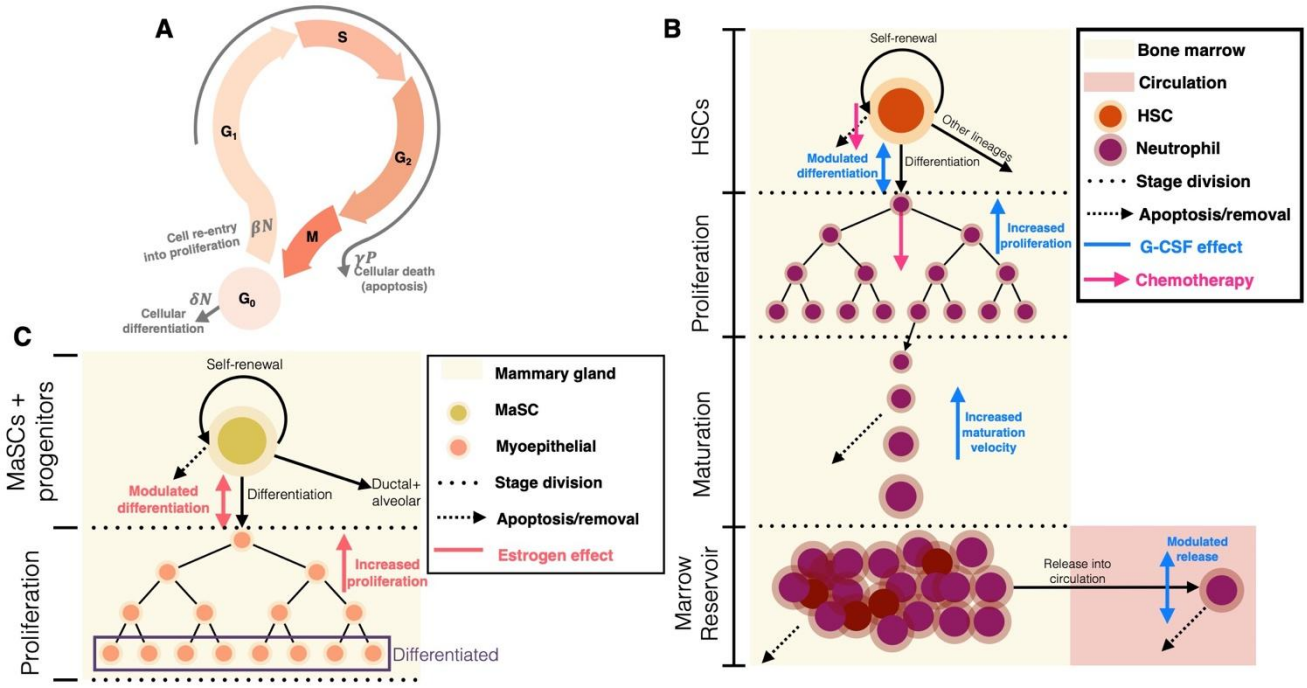

Figure 1. Modelling stem cell systems. A) Schematic representation of the Mackey G0 stem cell model [30]. Labels indicate the passage through the cell cycle (G_0, G_1, S, G_2, and M). Reproduced with permission from [33]. B) Schematic representation of our previous granulopoiesis model [7], with hematopoietic stem cell model based on the model in A. Hematopoietic stem cells self-renew or differentiate into neutrophils or other lineages. After differentiation into the neutrophil lineage, they undergo a period of exponential expansion before maturing. Mature neutrophils reside in the bone marrow reservoir before egressing out into circulation. These processes are modulated by the cytokine granulocyte colony-stimulating factor (G-CSF), as indicated. Reproduced under Creative Commons license from [12]. C) Schematic of the mammary stem cell model developed here. Based on A and B, MaSCs self-renew to maintain population numbers, and differentiate into alveolar, ductal, or myoepithelial lines. After differentiating, cells undergo a period of exponential expansion, regulated by estrogen concentrations to become myoepithelial cells.

where f_Q represents the maximal rate of self-renewal, θ_2 is the concentration of SCs eliciting 50% of the maximal rate, and s_2 is a Hill coefficient that regulates the slope of the stimulatory effects curve.

Decreases in the concentration of MaSCs arise in two ways: by cells entering mitosis at rate $\beta(Q)$ or through their exit from the compartment to begin differentiation toward mature cells. We modelled the second scenario as dependent on the concentration of free estrogen by

$$\kappa(E_f) = \kappa^* + (\kappa^* - \kappa^{min})\left[\frac{E_f^{s_1} - (E_f^*)^{s_1}}{E_f^{s_1} + (E_f^*)^{s_1}}\right]. \tag{3}$$

Here κ^* represents the homeostatic rate of differentiation, κ^{min} the minimal rate of differentiation (included to ensure that differentiation continues in absence of estrogen, which is known to occur through signalling by other hormones including progesterone and prolactin), E_f^* is the homeostatic

concentration of free estrogen, and s_1 is the Hill coefficient regulating the slope of the effect curve. In this model we kept the assumption of Craig et al. [7], where κ^* is found at the middle point between its maximum and minimum values. It is therefore defined as $1/2(\kappa^{max} + \kappa^{min})$ which implies the supremum of $\kappa(E_f)$ is $\kappa^{max} = 2\kappa^* - \kappa^{min}$. We chose to use a Hill function to model both the rate of differentiation in Eq (3) and the rate of proliferation (see Eq (6) below) given that there are limits to the physiological capacity of cells to divide. This implies that both of these rates will saturate at high concentrations of stimulation. Further, since estrogen is but one of a host of hormones acting in this system, the minimal concentration takes into account that there are overlapping functions for these signalling molecules and that differentiation/proliferation continues in absence of estrogen [31].

We discounted differentiation into alveolar and ductal cells and focused solely on mammary myoepithelial cell production. Thus, after differentiating, MaSCs become myoepithelial progenitor cells and undergo a period of exponential expansion lasting τ_M days. To quantify the concentration of cells produced during this proliferative period, we introduced a second amplification term specific to the myoepithelial population defined by

$$A_M(\mathrm{t}) = \exp\left[\int_{t-\tau_M}^{t} \eta_P\left(E_f(s)\right) ds\right]. \tag{4}$$

This amplification term accounts for proliferation occurring at rate η_P, regulated by free estrogen E_f, during which cells undergo mitosis for τ_M days. To facilitate computational implementation, we differentiated Eq (4) using Leibniz's rule to obtain the following differential equation

$$\frac{\mathrm{dA_M(t)}}{\mathrm{dt}} = \mathrm{A_M(t)}\left[\eta_\mathrm{P}\left(\mathrm{E}_f(\mathrm{t})\right) - \eta_\mathrm{P}\left(\mathrm{E}_f(\mathrm{t}-\tau_\mathrm{M})\right)\right], \tag{5}$$

as in previous work [7]. The rate of mitosis was described by

$$\eta_P\left(E_f(\mathrm{t})\right) = \eta_P^* + \left(\eta_P^* - \eta_P^{min}\right)\frac{b_P}{E_f^*}\left(\frac{E_f(t) - E_f^*}{E_f(t) - b_P}\right), \tag{6}$$

where η_P^* is the homeostatic rate of proliferation, η_P^{min} is the minimal rate of proliferation, and b_P is the half-maximal concentration of estrogen. Mature myoepithelial cells were modelled to apoptose at rate γ_M.

Taken together, the complete model of the mammary myoepithelial cell differentiation program regulated by estrogen is described by

$$\frac{dQ}{dt} = A_Q(t)\beta\left(Q\left(t-\tau_Q\right)\right)\mathrm{Q}\left(t-\tau_Q\right) - \left(\kappa\left(E_f(t)\right) + \beta\left(Q(t)\right)\right)\mathrm{Q}(t), \tag{7}$$

$$\frac{dM}{dt} = A_M(t)\kappa\left(E_f(t-\tau_M)\right)\mathrm{Q}(t-\tau_M) - \gamma_M\mathrm{M}(t). \tag{8}$$

2.2. Population pharmacokinetic and QSP model of estrogen

Pharmacokinetic (PK) models describe drug concentrations over time, and are generally

compartmental, describing sections of the body in which the drug readily distributes and can therefore be summarized as having a single concentration at any given time. Population PK (PopPK) models aim to characterize variations in PK parameters within a given population using nonlinear mixed-effect models, which are statistical models that contain both fixed (mean) and random (interindividual) effects. From data, a structural model (the compartmental PK model) is established by finding the best estimates for the population parameter value (fixed effect) with reference to the variation within the sample population (random) effects. Parameters are then represented as an exponentially distributed random variable by a singular fixed effect (usually referred to as θ) with noise parameters denoting the variability between individual subjects and the population value. These random effects are generally assumed to be normal or log-normal with zero mean and variance Ω^2. Parameters may also have covariate effects – additional variables that account for some of the variation of said parameter, and are particularly relevant in pharmaceutical models as drug kinetics are known to be determined by a variety of biological factors often modulated by specific patient characteristics e.g., age, body weight, habits, etc.

To account for the effects of interindividual variability (IIV) in estrogen pharmacokinetics, we leveraged a previous PopPK model [34] that characterized the pharmacokinetics of ethinyl estradiol (EE), an estrogen medication which, alongside drospirenone, is one of the active compounds in combined oral contraceptives. In the Reif et al. study [34], n = 1109 healthy young women received EE 20 μg and drospirenone 3 mg as a combined oral contraceptive. Patients were randomized to receive three different cyclical regimens

(1) Flexible (n = 671): one tablet per day for a flexible number of cycles (between 3 to 13 cycles). The minimum duration of active treatment was 24 days ('mandatory phase'). Afterwards, the cycle could continue up to 120 days or until the subject experienced 3 consecutive days of breakthrough bleeding or spotting ('flexible phase');
(2) Conventional (n = 224): subjects received one dosage per day for 13 cycles. Each cycle comprised 24 days of active hormonal intake followed with 4 days of placebo tablets;
(3) Fixed (n = 214): subjects received one dose per day for 3 cycles; each cycle comprised 120 days of active hormone intake followed by 4 days of placebo tablet;

during which four blood samples were collected from all subjects in the study, two during week 3, and two during week 27. EE concentrations were determined by immunoassay with a lower limit of quantification of 5.0 pg/ml. Data on age, BMI, body weight (BW), and cigarette and alcohol consumption were collected at both weeks, and data was then fit by means of nonlinear mixed-effects modeling using the NONMEM software package to construct the compartmental PK model.

In the analysis by Reif et al. [34], the pharmacokinetics of estradiol were characterized by a three-compartment population PK model with linear elimination given by

$$\begin{aligned}
\frac{dA_1}{dt} &= -\left(\frac{CL}{V_1} + \frac{Q_2}{V_1} + \frac{Q_3}{V_1}\right)A_1 + \frac{Q_2}{V_2}A_2 + \frac{Q_3}{V_3}A_3, \\
\frac{dA_2}{dt} &= -\frac{Q_2}{V_2}A_2 + \frac{Q_2}{V_1}A_1, \\
\frac{dA_3}{dt} &= -\frac{Q_3}{V_3}A_3 + \frac{Q_3}{V_1}A_1,
\end{aligned}$$

where A_1, A_2, A_3 represent the amount of EE in the central (1) and two peripheral (2,3) compartments. CL denotes clearance (in units L/h), Q_2 the intercompartmental clearance between compartments 1 and 2 (in units L/h), Q_3 the intercompartmental clearance between compartments

1 and 3 (in units L/h), V_1 the central volume of distribution (in units L), V_2 the volume of distribution in compartment 2 (in units L), and V_3 is the volume of distribution in compartment 3 (in units L). Note that intercompartmental transit can also be represented by rate constants $k_{ij} = \frac{Q_{ij}}{V_i}$, where Q_{ij} is the intercompartmental clearance between compartments *i* and *j* and V_i is the volume of distribution in compartment *i*. Reif et al. also found covariate relationships on the bioavailability F defined by

$$F = F_{week\,3}(1 + F_{week\,27}OCA),$$

where $OCA = \begin{cases} 0 & if\ week\ 3 \\ 1 & else \end{cases}$

and

$$CL = TVCL \exp(ETA_{CL})\,(CO2)(CO1)$$

for clearance, where $CO1 = 1 + CL_{AGE}(\log(AGE) - \log(24))$ and $CO2 = (1 + CL_{BW}(BW - 62))$ are covariates of age and body weight (kg) on clearance. Parameter values of the PopPK model are provided in Table 1.

Table 1. Population pharmacokinetic parameters from Reif et al. [34].

Parameter (units)	Interpretation	Estimate	%RSE
Fixed Effects			
		θ	
$TVCL/F$ (L/h)	Oral clearance	25.3	1.24
V_1/F (L)	Apparent volume of central compartment	23.9	13.6
V_2/F (L)	Apparent volume of second compartment	1,330	3.62
V_3/F (L)	Apparent volume of third compartment	23.9	-
Q_2/F (L/h)	Intercompartmental clearance to Compartment 2	52.9	7.01
Q_3/F (L/h)	Intercompartmental clearance to Compartment 3	8.49	34.3
k_a (1/h)	Absorption rate constant	0.295	6.98
$F_{week\,3}$	Relative bioavailability in week 3	1	-
$DF_{week\,27}$ (%)	Difference in relative bioavailability in week 27 to week 3	8.15	11.0
$ALAG$ (h)	Lag time	0.353	2.78
Fixed covariate effects			
CL_{age} (%/ln(year))	Influence of age on clearance	20.8	29.1
CL_{BW} (%/kg)	Influence of body weight on clearance	0.591	20.1
Interindividual Variability			
		%CV	
IIV_{CL}	IIV of clearance	33.4	2.65
Residual Error			
Proportional error	Proportional residual error	24.4	1.38

A downside of compartmental PK models is their reduced connection to known physiology. To improve physiological realism, we integrated the Reif et al. PopPK model [34] into our previous

mechanistic PK framework to further track the concentrations of free and bound estrogen in the plasma [7]. This integrated model is given by

$$\frac{dE_f}{dt} = E_{prod} - k_{ren}\,\mathrm{E}_f(t) - k_b\big((Q+M)V - E_b(t)\big)E_f(t)^{Pow} + k_u E_b(t) - (k_{12}+k_{13})E_f + k_{21}E_2 + k_{31}E_3, \tag{9}$$

$$\frac{dE_b}{dt} = -k_{int}\,E_b(t) + k_b\big((Q+M)V - E_b(t)\big)E_f(t)^{Pow} - k_u E_b(t), \tag{10}$$

$$\frac{dE_2}{dt} = k_{12}E_f - k_{21}E_2, \tag{11}$$

$$\frac{dE_3}{dt} = k_{13}E_f - k_{31}E_3, \tag{12}$$

where E_f and E_b are free and bound estrogen concentrations, E_{prod} is the rate of endogenous estrogen production, k_b and k_u are the respective binding and unbinding rates, k_{int} is the internalization rate of bound cytokine, k_{ren} is the elimination rate, pow is a stoichiometric constant relating the number of estrogen molecules per receptor, V is a scaling factor given by

$$V = \hat{p}E_{MW}K10^n,$$

with $\hat{p}$ a constant relating the stoichiometry between estrogen and its receptor, K the number of estrogen receptors on a cell's surface, and 10^n is a factor correcting for cellular units. In the equation above, E_{MW} represents the molecular weight of estrogen which was calculated by dividing its molar mass (MM) by Avogadro's number. The remaining terms in Eqs (3), (5), and (6) correspond to a reconfiguration of the PopPK model above to be expressed in concentrations in the central (E_f), second (E_2), and third (E_3) compartments, with $k_{12} = Q_2/V_1$, $k_{21} = Q_2/V_2$, $k_{13} = Q_3/V_1$, $k_{31} = Q_3/V_3$, and $k_{ren} = CL/V_1$, with CL representing linear (renal) clearance.

2.3. Parameter estimation

Since our model was constructed from physiological mechanisms, a majority of the QSP model's parameters were estimated directly from the literature. In absence of direct information about mammary stem cells, we made an assumption of a parallel between MaSCs and HSCs and leveraged our previous work in Craig et al. [7] as proof-of-concept. Estrogen PopPK parameters were obtained directly from the estimates in Supplementary Table 1 in Reif et al. [34] (Table 1). Any remaining parameters were calculated to ensure homeostasis in our model as follows. We calculated θ_2 from the equation for the self-renewal of mammary stem cells $\beta\big(Q(t)\big)$ by

$$\theta_2 = \sqrt[S_2]{\frac{Q^{*S_2}\beta^*}{f_Q - \beta^*}} = \frac{Q^*\beta^{*\frac{1}{S_2}}}{(f_Q - \beta^*)^{\frac{1}{S_2}}}. \tag{13}$$

Setting Q^* to its estimated homeostatic value (Table 2), we calculated the homeostatic rate of differentiation as

$$\kappa^* = \beta^*\left(A_Q^* - 1\right). \tag{14}$$

Similarly, the homeostatic amplification factor for myoepithelial cells was calculated from Eq (8) by

$$A_M^* = \frac{M^*\gamma_M}{\kappa^* Q^*}. \tag{15}$$

Here, A_M^* quantifies the effective amplification of progenitor cells after differentiation given by the ratio of the rate cells leave the progenitor compartment (through $M^*\gamma_M$) to the rate cells enter (i.e. $\kappa^* Q^*$) at homeostasis. Assuming there are 10 divisions between stem cells and terminally differentiated myoepithelial cells [35], the number of proliferating cells is calculated explicitly as $\kappa^* Q^* 2^{10}$, thus

$$\eta_P{}^* = \frac{(A_M^* - 1)}{(10)(2^{10})}. \tag{16}$$

The homeostatic concentration of bound estrogen (E_b^*) was calculated directly from Eq (10) using

$$E_b^* = \frac{(k_{12} + k_{13})E_f^* - k_{21}E_2^* - k_{31}E_3^* - E_{prod} + k_{ren}E_f^* + k_b(Q^* + M^*)V\left(E_f^*\right)^{Pow}}{k_u + k_b\left(E_f^*\right)^{Pow}}, \tag{17}$$

and the rate of estrogen production from Eq (9)

$$E_{prod} = k_{ren}E_f^* + k_b\left((Q^* + M^*)V - E_b^*\right)\left(E_f^*\right)^{Pow} - k_u E_b^* + (k_{12} + k_{13})E_f^* - k_{21}E_2^* - k_{31}E_3^*. \tag{18}$$

Lastly, the homeostatic concentration of estrogen in the second and third compartments, E_2^* and E_3^*, were estimated by setting Eqs (11) and (12) to 0, given that E_f^* has been previously estimated [36].

$$E_2^* = \frac{\mathrm{k_{12}E_f^*}}{\mathrm{k_{21}}}, \tag{19}$$

$$E_3^* = \frac{k_{13}E_f^*}{k_{31}}. \tag{20}$$

2.4. Model simulations

Model simulations were carried out using the *ddesd* function in Matlab 2020a. Unless otherwise noted, initial values of all variables were set to their homeostatic values, indicated by superscript *.

2.5. Sensitivity analysis

To investigate the effects of variability in parameters on model predictions, we used partial rank correlation coefficient (PRCC) analysis to assess uncertainty and sensitivity on the multi-dimensional parameter space [37]. For each investigated parameter, we generated a uniform distribution around the mean (or fixed) parameter value. This set of parameter values was then included to create a Latin hypercube sampling (LHS) scheme. We next simulated and recorded the

relevant outputs of the model (specifically $min(Q(t))$ and $max(M(t))$) using the samples in the LHS scheme. Finally, we calculated the PRCC to establish correlations between parameters and the model outputs. These correlations were also assessed for statistical significance, given an α-level of 0.05. For this analysis, we adapted the approach and code from Marino et al. [37].

3. Results

3.1. Estimated and calculated parameter values of myoepithelial cell production by mammary stem cells regulated by estrogen

Physiological and mechanistic PK parameter values were estimated from literature sources or through calculations to ensure homeostasis in the model (see Methods). Table 2 and Table 3 summarize all parameter values in these model components.

Table 2. Physiological model parameter values.

Parameter	Value	Units	Definition	Reference
τ_Q	24	hours	Length of MaSC cell cycle	[38]
τ_M	10	days	Duration of proliferative phase	[39]
γ_Q	0.1	1/day	MaSC apoptotic rate during mitosis	[40]
A_Q^*	1.8097	--	Amplification factor	[7]
β^*	0.043	1/day	Stem cell rate of self-renewal	[7]
f_Q	8	1/day	Maximal stem cell renewal	[7]
θ_2	0.0809	10^6 cells/kg	Self-renewal half-effect concentration of MaSCs	Calculations from [7]
s_2	2	--	MaSC self-renewal Hill coefficient	[7]
s_1	1.5	--	MaSC differentiation Hill coefficient	[7]
κ^*	0.0348	1/day	Homeostatic rate of differentiation	Calculated (Eq (14))
κ^{min}	0.0174	1/day	Minimal rate of differentiation	[41]
Q^*	1.1	10^6 cells/kg	Homeostatic concentration of MaSC	[7]
A_M^*	27697	--	Myoepithelial proliferation amplification factor	Calculated (Eq (15))
$\eta_P{}^*$	2.7047	1/day	Homeostatic rate of proliferation of myoepithelial progenitors	Calculated (Eq (16))
$\eta_P{}^{min}$	1.3523	1/day	Minimal rate of proliferation of myoepithelial progenitors	[41]
b_p	0.022868	ng/ml	Half-maximal concentration of proliferation of myoepithelial progenitors	[7]
γ_M	0.113	1/day	Apoptotic rate of myoepithelial cells	[42]
K	4973	--	Number of estrogen receptors on MaSC/myoepithelial cell surface	[43]
V	0.0283	(ng/ml)/(10^9 cell/kg)	Conversion factor	Calculated
M^*	9.387	10^9 cells/kg	Homeostatic concentration of myoepithelial cells	[44]

Table 3. Additional estrogen pharmacokinetic parameter values.

Parameter	Value	Units	Definition	Reference
E_{prod}	3.2776	1/day	Rate of endogenous estrogen production	Calculated (Eq (18))
k_u	8.64	1/day	Rate of estrogen unbinding	[45]
k_b	23.53536	ng/ml/day	Rate of estrogen binding	[45]
k_{int}	43.2	1/day	Rate of estrogen internalization	[45]
k_{ren}	35.9335	1/day	Rate of renal clearance	Calculated
k_{12}	53.1213	1/day	Transit rate from 1st compartment to 2nd	[34]
k_{21}	0.9546	1/day	Transit rate from 2nd compartment to 1st	[34]
k_{13}	8.5255	1/day	Transit rate from 1st compartment to 3rd	[34]
k_{31}	8.5255	1/day	Transit rate from 3rd compartment to 1st	[34]
E_f^*	0.080	ng/ml	Homeostatic concentration of free estrogen	[36]
E_b^*	0.0093	ng/ml	Homeostatic concentration of bound estrogen	Calculated (Eq (17))
E_2^*	4.4519	ng/ml	Homeostatic estrogen concentration in 2nd compartment	Calculated (Eq (19))
E_3^*	0.08	ng/ml	Homeostatic estrogen concentration in 3rd compartment	Calculated (Eq (20))

3.2. Effects of repeated oral estrogen administration on myoepithelial cell production for an average individual

To provide a rationale for the use of estrogen as a means to induce myoepithelial differentiation of mammary stem cells, we first investigated the homeostatic regulation of the differentiation cascade. For this, we discounted interindividual variability, set all PK parameters to their fixed (θ) values (see Methods), and administered a single dose of 20μg of ethinyl estradiol (as in [34]). This single dose caused a small rise in myoepithelial cell counts, peaking around 10 days after administration, despite estrogen concentrations in most compartments returning to the homeostatic concentrations within 1-2 days (Figure 2).

These results suggest that a single 20 μg dose of estrogen does not steadily stimulate myoepithelial cell production, as myoepithelial cell concentrations peaked at only 1.06-times their homeostatic values. Therefore, we next interrogated the effects of exogenous, oral estrogen administration by simulating daily doses of 20μg of ethinyl estradiol (as in [34]). As expected, the concentrations of free estrogen in the central and peripheral compartments rapidly attained steady-state during the dosing period (Figure 3C-F). The rise in free estrogen concentrations induced continued differentiation of MaSC (Figure 3A), during which mammary myoepithelial cell concentrations nearly doubled, again peaking around 10 days after administration.

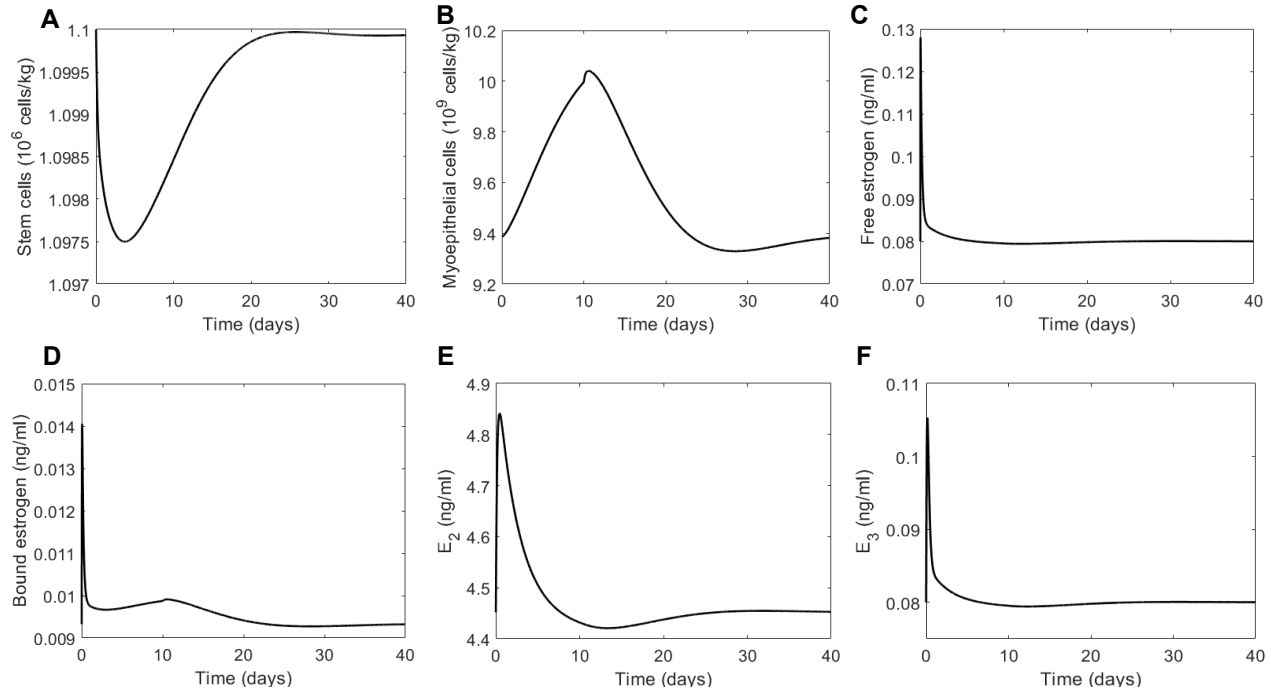

Figure 2. Single dose of oral estrogen weakly induces mammary stem cell differentiation into myoepithelial cells. Effects of a single $20\mu g$ dose of ethinyl estradiol on A) mammary stem cells, B) myoepithelial cells, C) free estrogen, D) bound estrogen, E) estrogen concentrations in the second compartment, and F) estrogen concentrations in the third compartment in an average individual.

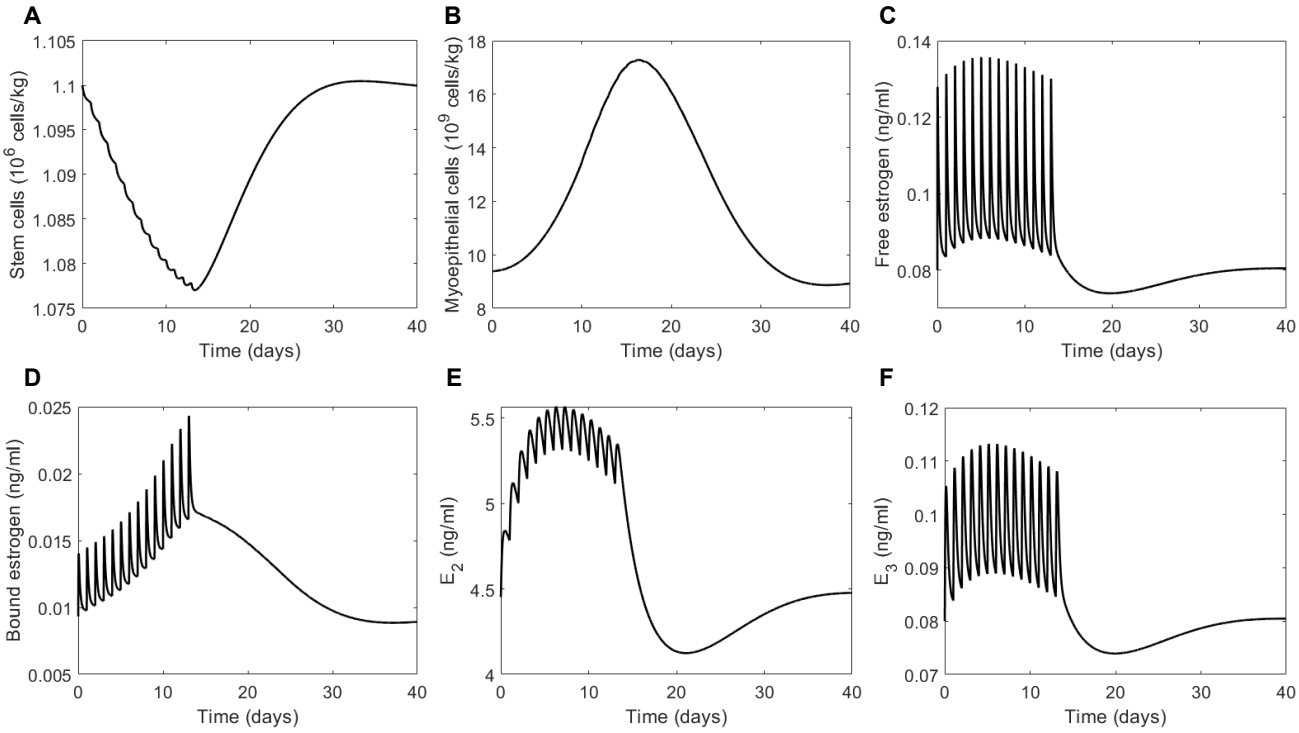

Figure 3. Multiple administrations of oral estrogen stimulate mammary myoepithelial production. Effects of a 14 repeated 20 μg doses of ethinyl estradiol on A) mammary stem cells, B) myoepithelial cells, C) free estrogen, D) bound estrogen, E) estrogen concentrations in the second compartment, and F) estrogen concentrations in the third compartment in an average individual.

3.3. Effects of pharmacokinetic variability on mammary stem cell differentiation

Up to this point, we have explored the effects of estrogen stimulation on mammary stem cell differentiation for a single average individual. However, given the variability estimated in our adapted PopPK model [34], we next sought to understand how population heterogeneity affects a QSP model of MaSC differentiation. We have previously shown that interindividual variability has little to no effect on pharmacokinetic and pharmacodynamic variability in a similar model of hematopoietic differentiation, likely due to the inherent heterogeneity captured in mechanistic QSP models [46]. Therefore, to study the effects of interindividual variability in the context of mammary stem cell differentiation, we generated 300 virtual patients by sampling from a normal distribution of body weights (BWs) centered around the mean BW of 63 kg reported in Reif et al. [34], with a standard deviation of 8.6 kg informed by two recent surveys carried out by the NCD Risk Factor Collaboration [47,48]. We chose to generate virtual patients using body weight as it was found to be a covariate of clearance in the original PopPK analysis [34]. The effects of IIV on clearance (also estimated by Reif et al.) were also investigated and found to be consistent with the results of the body weight analysis. Normality in the generated body weights was confirmed using Shapiro-Wilk and Shapiro-Francia normality tests (p-value of 0.5565 at the 5% significance level, see Figure 4) [49].

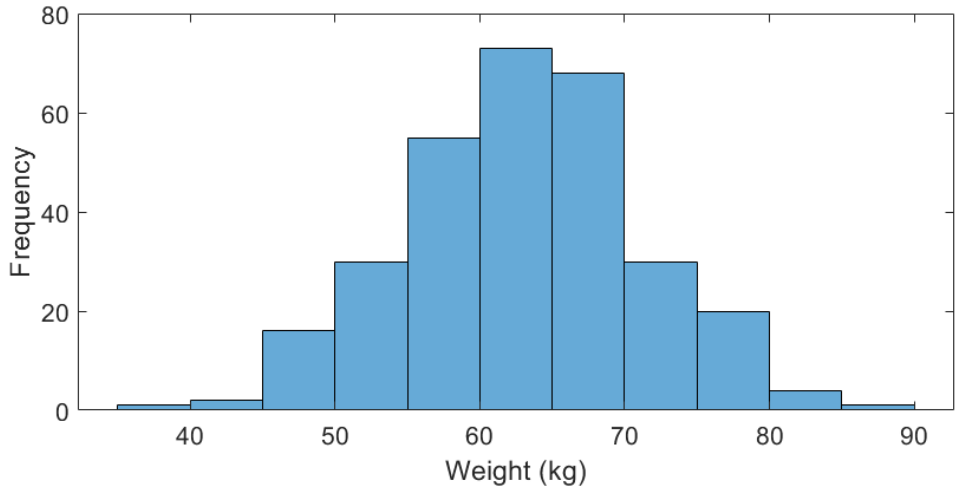

Figure 4. Distribution of body weights in generated virtual population. Virtual patients were generated by sampling from a normal distribution with mean body weight as reported in Reif et al. [34] and standard deviation informed by population sampling [47,48].

We next again simulated a single oral dose for each virtual patient to quantify the degree to which pharmacokinetic variability affected our model's predictions. Across both cellular populations and all estrogen compartments, we observed no effect of pharmacokinetic variability on our predictions (Figure 5).

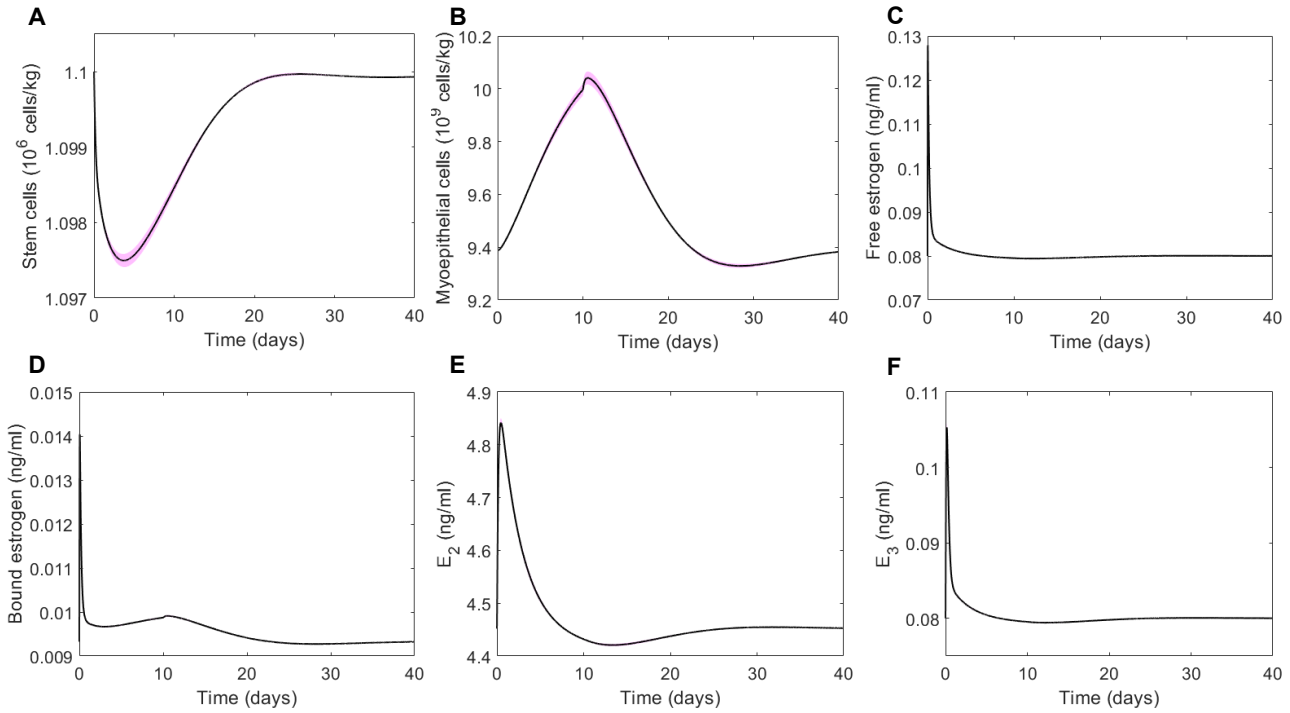

Figure 5. Pharmacokinetic variability has little to no impact on QSP model predictions in cohort of 300 virtual patients after single administration of estrogen. Effects of a single 20 μg dose of ethinyl estradiol on A) mammary stem cells, B) myoepithelial cells, C) free estrogen, D) bound estrogen, E) estrogen concentrations in the second compartment, and F) estrogen concentrations in the third compartment in a virtual cohort of 300 patients. Virtual patients were generated by sampling from a distribution of bodyweight, a covariate for clearance in the PopPK model [34] (see Methods). Black solid lines: mean model prediction in cohort of 300 virtual patients; shaded pink regions: range of responses in virtual patient cohort.

These results were further recapitulated when we considered repeated daily doses in the same virtual population. This additional heterogeneity had very little discernable impact on either the MaSCs or the myoepithelial cells (Figure 6A and Figure 6B), and low impact on any of the estrogen compartments (Figure 6C-F). This is notable given that the bound estrogen concentrations drive all the pharmacodynamic effects in our model and, despite observing no IIV impact on bound estrogen concentrations, there are nonetheless observable (but small) amounts of heterogeneity in the MaSC and myoepithelial populations after repeated administrations.

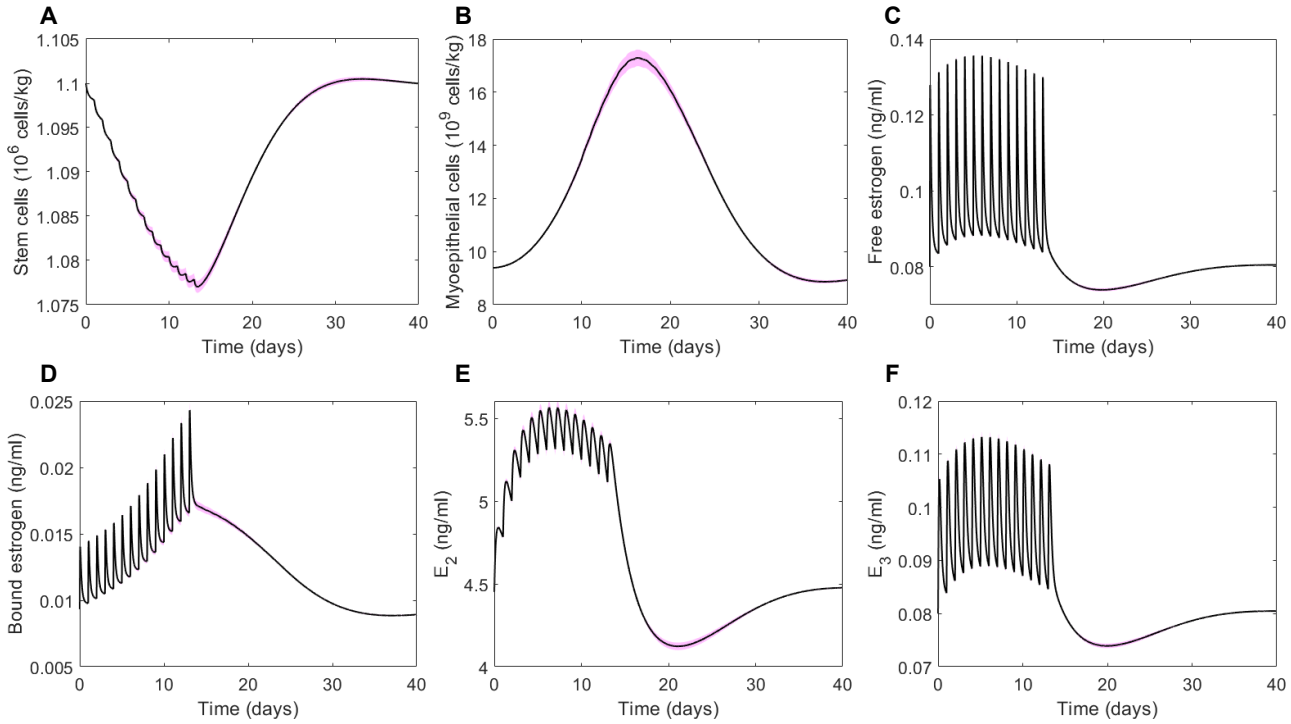

Figure 6. Pharmacokinetic variability has little to no impact on QSP model predictions in cohort of 300 virtual patients after repeated daily doses of estrogen. Effects of 14 repeated 20 μg doses of ethinyl estradiol on A) mammary stem cells, B) myoepithelial cells, C) free estrogen, D) bound estrogen, E) estrogen concentrations in the second compartment, and F) estrogen concentrations in the third compartment in a virtual cohort of 300 patients. Virtual patients were generated by sampling from a distribution of bodyweight, a covariate for clearance in the PopPK model [34] (see Methods). Black solid lines: mean model prediction in cohort of 300 virtual patients; shaded pink regions: range of responses in virtual patient cohort.

3.4. Sensitivity analysis

Sensitivity of model predictions to parameter variability was assessed using partial rank correlation coefficients (PRCC), as described in the Methods. To perform the PRCC analysis, we included several of our model parameters to assess their effect on the stem cell and myoepithelial cell populations after the introduction of a single dose of estradiol. Physiological parameters included were the time delays (τ_Q and τ_M) and death rates (γ_Q and γ_M) for both cell populations, in addition to β^* and b_p to assess effects related to mitosis and proliferation. Further, since our virtual population was generated from body weights that impact on the rate of renal clearance, we also investigated the effects of variability in k_{ren} to assess the degree to which our model is sensitive to this important parameter.

We generated our LHS scheme by creating uniform distributions around mean estimated parameter values (Tables 1–3), with maximum and minimum values for the distributions set to be the mean value $\pm$25%. With a sample size of 100, we ran the PRCC analysis for the effect on the minimum stem cell concentration ($min\ Q(t)$) and the maximum myoepithelial cell concentration ($max\ M(t)$).

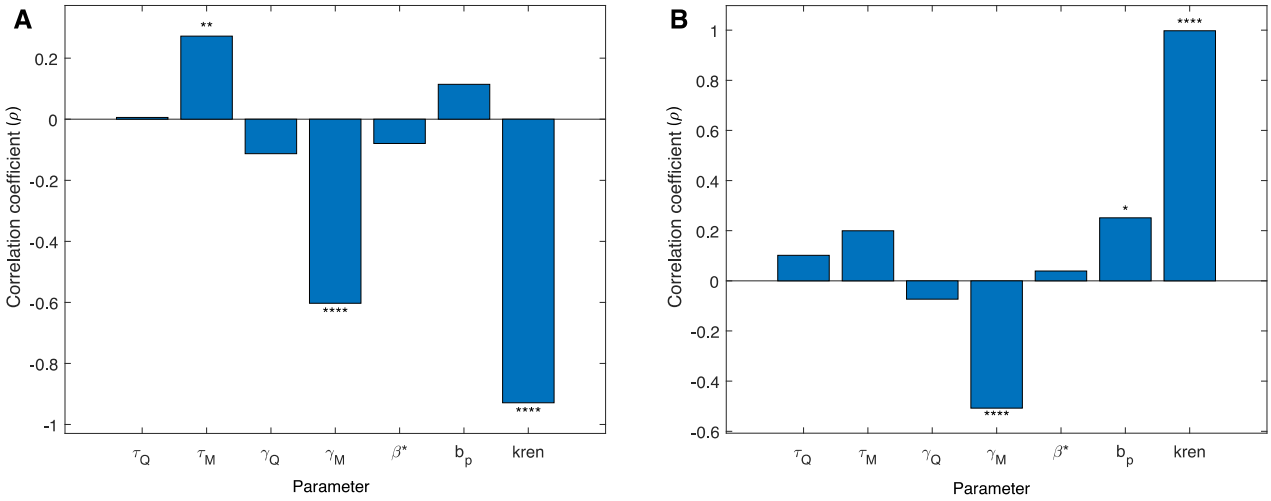

Figure 7. Individual correlation coefficient for each parameter with its p-value significance from the PRCC analysis. The sensitivity of model predictions to parameter changes was assessed using partial rank correlation coefficient analysis and Latin hypercube sampling. Correlation coefficients between each parameter and A) the minimum stem cell concentration and B) the maximum myoepithelial cell concentration after a single dose of estradiol. * indicates a p-value smaller or equal to 0.05, ** p-value smaller or equal to 0.01 but greater than 0.001, and **** a p-value smaller or equal to 0.0001 (calculated at a level of significance of $\alpha = 0.05$).

As shown in Figure 7, renal clearance was found to be the most sensitive parameter in our model, strongly impacting on both minimal MaSC and maximal mature cell concentrations. This analysis therefore further supports the use of body weight to generate the virtual cohort, as variations in bodyweight directly affect k_{ren}.

4. Discussion

Mammary stem cell plasticity is a contributing factor to the development of aggressive breast cancer subtypes. A quantitative understanding of the regulation of the mammary cell differentiation program controlled by estrogen and other hormones is needed to provide insight into how this regulation can be therapeutically targeted. In this work, we created a QSP model to study both mammary stem cell and myoepithelial cell populations and their regulation by estrogen signalling. Our model takes into account physiologically relevant pharmacokinetics by explicitly accounting for both unbound and bound estrogen concentrations in addition to empirically determined population pharmacokinetics.

By investigating the effects of single and repeated oral ethinyl estradiol doses in an average patient, we demonstrated the small effect of a single dose on both cell populations included in our model. However, in the two-week regimen of daily doses, we observed a doubling in the concentration of mammary myoepithelial cells, suggesting that repeated stimulation is required to sustainably induce increased MaSC differentiation into this cell type. Since the process of dedifferentiation relies on hormones such as estrogen and could therefore be theoretically affected by an increase in estrogen concentrations, it has been proposed that forcing cancer cells to differentiate can ultimately reduce cancer aggressivity and proliferation capacities. Thus, our results support

continued work investigating the regulation of the mammary stem cell niche.

Importantly, we also observed that PK variability in clearance provided little to no impact on our QSP model by generating a population of 300 virtual patients based on the integrated population pharmacokinetic model. In this cohort, both the single dose and repeated administrations over 14 days did not show meaningful variation in cell population and even less variation in the estrogen compartments. This suggests that sources of empirically determined PK variability may be accounted for within QSP models constructed from physiological first principles. Indeed, PK variability was shown to insignificantly affect our model predictions. As our PRCC analysis showed, the effect of renal clearance was found to be most significantly correlated with changes in model output. However, other physiological parameters were also found to be sensitive, and future studies should explore combinations of physiological parameters to assess their effects on driving heterogeneity in our model. Interestingly, we have previously shown similar results when integrating PopPK/PD estimates into our similar model of neutrophil production [46]. There, estimated pharmacodynamic variability had a much larger impact on heterogeneous model outcomes than interindividual variability estimated through PopPK analyses, as in the present study. It should also be noted that we did not explore the effects of age or interoccasion variability, which was found in Reif et al. [34] to be related to heterogeneity in clearance. Our results would be further strengthened by improved estimates of MaSC parameters.

As noted, mammary stem cells can additionally differentiate into alveolar and ductal cell types, and the MaSC differentiation program is regulated by other hormones including progesterone and prolactin. Future studies will incorporate these considerations to increase the physiological realism and applicability of our system, and focus on experimental validation. Nonetheless, our approach establishes a theoretical framework with which we can explore how dysregulated mammary stem cell signalling can lead to malignancy and, as such, is an important element of preclinical and translational studies as part of a precision medicine in breast cancer.

Acknowledgments

JLSR was supported by ISM and CAMBAM graduate fellowships. All authors were supported by NSERC Discovery Grant RGPIN-2018-04546 (MC).

Conflict of interest

The authors have no conflicts of interest to declare.

References

1. G. C. Sieck, Physiology in perspective: stem cells and regenerative physiology, *Physiology,* **33** (2018), 14–15.
2. M. C. Mackey, Cell kinetic status of hematopoietic stem cells, *Cell Prolif.,* **34** (2001), 71–83.
3. J. Till, E. McCullogh, A direct measurement of the radiation sensitivity of normal mouse bone marrow cells, *Radiat. Res.,* **14** (1961), 213–222.
4. H. Lee-Six, N. F. Øbro, M. S. Shepherd, S. Grossmann, K. Dawson, M. Belmonte, Population dynamics of normal human blood inferred from somatic mutations, *Nature*, **561** (2018), 473–478.

5. M. S. Krieger, J. M. Moreau, H. Zhang, M. Chien, J. L. Zehnder, M. Craig, A blueprint for identifying phenotypes and drug targets in complex disorders with empirical dynamics, *Patterns*, **1** (2020), 100138.
6. M. Craig, A. R. Humphries, F. Nekka, J. Belair, J. Li, M. C. Mackey, Neutrophil dynamics during concurrent chemotherapy and G-CSF administration: mathematical modelling guides dose optimisation to minimise neutropenia, *J. Theor. Biol.*, **385** (2015), 77–89.
7. M. Craig, A. R. Humphries, M. C. Mackey, A mathematical model of granulopoiesis incorporating the negative feedback dynamics and kinetics of G-CSF/neutrophil binding and internalisation, *Bull. Math. Biol.*, **78** (2016), 2304–2357.
8. L. E. Friberg, M. O. Karlsson, Mechanistic models for myelosuppression, *Invest. New Drugs*, **21** (2003), 183–194.
9. M. Scholz, C. Engel, M. Loeffler, Modelling human granulopoiesis under polychemotherapy with G-CSF support, *J. Math. Biol.*, **50** (2005), 397–439.
10. V. Vainstein, Y. Ginosar, M. Shoham, D. O. Ranmar, A. Ianovski, Z. Agur, The complex effect of granulocyte colony-stimulating factor on human granulopoiesis analyzed by a new physiologically-based mathematical model, *J. Theor. Biol.*, **235** (2005), 311–327.
11. S. Alfonso, A. L. Jenner, M. Craig, Translational approaches to treating dynamical diseases through in silico clinical trials, *Chaos An Interdiscip. J. Nonlinear Sci.*, **30** (2020), 123128.
12. M. Craig, Towards quantitative systems pharmacology models of chemotherapy-induced neutropenia, *CPT Pharmacometrics Syst. Pharmacol.*, **6** (2017), 293–304.
13. P. Sorger, S. R. B. Allerheiligen, D. Abernethy, R. B. Altman, K. L. Brouwer, A. Califano, et al. Quantitative and systems pharmacology in the post-genomic era: new approaches to discovering drugs and understanding therapeutic mechanisms, *An NIH white paper by the QSP workshop group*, **48** (2011), 1–47.
14. A. L. Jenner, T. Cassidy, K. Belaid, M. C. Bourgeois-Daigneault, M. Craig, In silico trials predict that combination strategies for enhancing vesicular stomatitis oncolytic virus are determined by tumor aggressivity, *J. Immunother. Cancer,* **9** (2021), e001387.
15. T. Cassidy, M. Craig, Determinants of combination GM-CSF immunotherapy and oncolytic virotherapy success identified through in silico treatment personalization, *PLOS Comput. Biol.*, **15** (2019), e1007495.
16. H. Wang, O. Milberg, I. H. Bartelink, P. Vicini, B. Wang, R. Narwal, et al. In silico simulation of a clinical trial with anti-CTLA-4 and anti-PD-L1 immunotherapies in metastatic breast cancer using a systems pharmacology model, *R. Soc. Open Sci.*, **6** (2020), 190366.
17. H. Ma, H. Wang, R. J. Sové, J. Wang, C. Giragossian, A. S. Popel, Combination therapy with T cell engager and PD-L1 blockade enhances the antitumor potency of T cells as predicted by a QSP model, *J. Immunother. Cancer,* **8** (2020), e001141.
18. O. Milberg, C. Gong, M. Jafarnejad, I. H. Bartelink, B. Wang, P. Vicini, et al. A QSP Model for Predicting Clinical Responses to Monotherapy, Combination and Sequential Therapy Following CTLA-4, PD-1, and PD-L1 Checkpoint Blockade, *Sci. Rep.*, **9** (2019), 1–17.
19. S. Soufsaf, P. Robaey, G. Bonnefois, F. Nekka, J. Li, A quantitative comparison approach for methylphenidate drug regimens in attention-deficit/hyperactivity disorder treatment, *J. Child Adolesc. Psychopharmacol.*, **29** (2019), 220–234.
20. J. E. Visvader, J. Stingl, Mammary stem cells and the differentiation hierarchy: current status and perspectives, *Genes Dev.*, **28** (2014), 1143–1158.

21. R. G. Mehta, M. Hawthorne, R. R. Mehta, K. E. Torres, X. Peng, D. L. McCormick, et al. Differential Roles of ERα and ERβ in Normal and Neoplastic Development in the Mouse Mammary Gland, *PLoS One*, **9** (2014), e113175.
22. M. Romagnoli, S. Cagnet, A. Chiche, L. Bresson, S. Baulande, P. de la Grange, et al. Deciphering the Mammary Stem Cell Niche: A Role for Laminin-Binding Integrins, *Stem Cell Reports*, **12** (2019), 831–844.
23. Canadian Cancer Statistics Advisory Committee, *Canadian Cancer Statistics*, Toronto, 2018.
24. M. Fedele, L. Cerchia, G. Chiappetta, The epithelial-to-mesenchymal transition in breast cancer: Focus on basal-like carcinomas, *Cancers (Basel)*, **9** (2017), 134.
25. V. M. López-Ozuna, I. Y. Hachim, M. Y. Hachim, J. J. Lebrun, S. Ali, Prolactin modulates TNBC aggressive phenotype limiting tumorigenesis, *Endocr. Relat. Cancer,* **26** (2019), 321–337.
26. G. Dontu, D. El-Ashry, M. S. Wicha, Breast cancer, stem/progenitor cells and the estrogen receptor, *Trends Endocrinol. Metab.*, **15** (2004), 193–197.
27. F. Liu, A. Pawliwec, Z. Feng, Z. Yasruel, J. J. Lebrun, S. Ali, Prolactin/Jak2 directs apical/basal polarization and luminal linage maturation of mammary epithelial cells through regulation of the Erk1/2 pathway, *Stem Cell Res.*, **15** (2015), 376–383.
28. A. Shams, J. Boudreault, N. Wang, et al. Prolactin receptor-driven combined luminal and epithelial differentiation in breast cancer restricts plasticity, stemness, tumorigenesis and metastasis, *Oncogenesis*, **10** (2021), 1–16.
29. V. M. Lopez-Ozuna, I. Y. Hachim, M. Y. Hachim, J. J. Lebrun, S. Ali, Prolactin Pro-Differentiation Pathway in Triple Negative Breast Cancer: Impact on Prognosis and Potential Therapy, *Sci. Rep.*, **6** (2016), 1–13.
30. M. C. Mackey, Unified hypothesis for the origin of aplastic anemia and periodic hematopoiesis, *Blood*, **51** (1978), 941–956.
31. S. Mallepell, A. Krust, P. Chambon, C. Brisken, Paracrine signaling through the epithelial estrogen receptor α is required for proliferation and morphogenesis in the mammary gland, *Proc. Natl. Acad. Sci.*, **103** (2006), 2196–2201.
32. S. Cristea, K. Polyak, Dissecting the mammary gland one cell at a time, *Nat. Commun.*, **9** (2018), 2473.
33. M. Brunetti, M. C. Mackey, M. Craig, Understanding Normal and Pathological Hematopoietic Stem Cell Biology Using Mathematical Modelling, *Curr. Stem Cell Reports*, (2021), 1–12.
34. S. Reif, N. Snelder, H. Blode, Characterisation of the pharmacokinetics of ethinylestradiol and drospirenone in extended-cycle regimens: population pharmacokinetic analysis from a randomised Phase III study, *J. Fam. Plan. Reprod. Heal. Care*, **39** (2013), e1–e13.
35. S. Huang, Gene expression profiling, genetic networks, and cellular states: An integrating concept for tumorigenesis and drug discovery, *J. Mol. Med.*, **77** (1999), 469–480.
36. J. B. Becker, K. J. Berkley, N. Geary, E. Hampson, J. P. Herman, E. Young, *Sex Differences in the Brain: From Genes to Behavior*, Oxford University Press, 2007.
37. S. Marino, I. B. Hogue, C. J. Ray, D. E. Kirschner, A methodology for performing global uncertainty and sensitivity analysis in systems biology, *J. Theor. Biol.*, **254** (2008), 178–196.
38. R. L. Sutherland, R. E. Hall, G. Y. N. Pang, E. A. Musgrove, C. L. Clarke, Effect of Medroxyprogesterone Acetate on Proliferation and Cell Cycle Kinetics of Human Mammary Carcinoma Cells, *Cancer Res.*, **48** (1988), 5084–5091.

39. R. B. Clarke, K. Spence, E. Anderson, A. Howell, H. Okano, C. S. Potten, A putative human breast stem cell population is enriched for steroid receptor-positive cells, *Dev. Biol.,* **277** (2005), 443–456.
40. C. H. Chang, M. Zhang, K. Rajapakshe, C. Coarfa, D. Edwards, S. Huang, et al. Mammary Stem Cells and Tumor-Initiating Cells Are More Resistant to Apoptosis and Exhibit Increased DNA Repair Activity in Response to DNA Damage, *Stem Cell Reports,* **5** (2015), 378–391.
41. J. Huang, P. Woods, D. Normolle, J. P. Goff, P. V. Benos, C. J. Stehle, et al. Downregulation of estrogen receptor and modulation of growth of breast cancer cell lines mediated by paracrine stromal cell signals, *Breast Cancer Res. Treat.,* **161** (2017), 229–243.
42. R. C. Humphreys, M. Krajewska, S. Krnacik, R. Jæger, H. Weiher, S. Krajewski, et al. Apoptosis in the terminal endbud of the murine mammary gland: A mechanism of ductal morphogenesis, *Development,* **122** (1996), 4013–4022.
43. R. Joseph, Y. L. Orlov, M. Huss, W. Sun, S. Li Kong, L. Ukil, et al. Integrative model of genomic factors for determining binding site selection by estrogen receptor-α, *Mol. Syst. Biol.*, **6** (2010), 1–13.
44. P. Eirew, J. Stingl, A. Raouf, G. Turashvill, S. Aparicio, J. T. Emerman, et al. A method for quantifying normal human mammary epithelial stem cells with in vivo regenerative ability, *Nat. Med.*, **14** (2008), 1384–1389.
45. J. J. Tyson, W. T. Baumann, C. Chen, A. Verdugo, I. Tavassoly, Y. Wang, et al. Dynamic modelling of oestrogen signalling and cell fate in breast cancer cells, *Nat. Rev. Cancer,* **11** (2011), 523–532.
46. M. Craig, M. Gonz ́alez-Sales, J. Li, F. Nekka, Impact of pharmacokinetic variability on a mechanistic physiological pharmacokinetic/pharmacodynamic model: a case study of neutrophil development, PM00104, and filgrastim, In: Toni B (Ed.), *Mathematical Sciences with Multidisciplinary Applications*, Springer, (2016), 91–112.
47. NCD Risk Factor Collaboration, Trends in adult body-mass index in 200 countries from 1975 to 2014: A pooled analysis of 1698 population-based measurement studies with 19.2 million participants, *Lancet,* **387** (2016), 1377–1396.
48. NCD Risk Factor Collaboration, A century of trends in adult human height, *Elife,* **5** (2016), 1–29.
49. A. BenSa ̈ıda, Shapiro-Wilk and Shapiro-Francia normality tests, *MATLAB Central File Exchange*, (2009).